



Oxidation and selective catalytic reduction of NO by propene over Pt and Pt:Pd diesel oxidation catalysts

M. Khosravi^a, C. Sola^a, A. Abedi^b, R.E. Hayes^{a,*}, W.S. Epling^{b,c}, M. Votsmeier^d

^a Department of Chemical and Materials Engineering, University of Alberta, Edmonton, AB, Canada

^b Department of Chemical Engineering, University of Waterloo, Waterloo, Ontario, Canada

^c Department of Chemical and Biomolecular Engineering, University of Houston, Houston, TX, United States

^d Umicore, Automotive Catalysts Division, Research and Development, Hanau, Germany

ARTICLE INFO

Article history:

Received 6 June 2013

Received in revised form 16 August 2013

Accepted 19 August 2013

Available online 28 August 2013

Keywords:

Nitrous oxide

Propene

Oxidation

Reduction

ABSTRACT

This paper describes an experimental and theoretical investigation of the selective catalytic reduction of NO by propene over two diesel oxidation catalysts. Both catalysts were commercial monolith samples of 400 CPSI with a PGM loading of 95 g/ft³. In one monolith the catalyst was platinum only, and in the other a bimetallic catalyst of 4:1 by mass platinum and palladium. Both catalysts showed some activity for the SCR reaction, although relatively large amounts of N₂O were also formed. Global kinetic models for the oxidation of propene, NO and the SCR reactions are developed. Several models from the literature were tested and compared. New models based on earlier work are proposed. A good agreement between experimental results and simulation was observed.

© 2013 Elsevier B.V. All rights reserved.

1. Introduction

Since the middle 1970s, exhaust gas emissions from automotive sources have been under increasingly strict government control. Early emissions reductions were met by engine modifications; however, although significant advances in engine design and operation have been made over the past years, catalytic converters are still required to eliminate exhaust gas such as carbon monoxide (CO), various oxides of nitrogen, (NO_x) and hydrocarbons (HC) [1]. For spark ignition (SI) engines with stoichiometric operating condition, the three-way catalytic converter (TWC) is the technology of choice. It is used to oxidize CO and HC and to reduce NO_x simultaneously. For diesel, compression ignition (CI) engines, which operate in the lean burn mode, the presence of a high concentration of oxygen in the exhaust gas makes it impossible to reduce the NO_x over a TWC. To overcome this problem, a combination of two types of converters in series is used. The first one, called diesel oxidation catalyst (DOC) [1] is responsible for oxidizing CO and HC. In this converter, NO is also oxidized to NO₂, although some nitrous oxide (N₂O) and nitrogen (N₂) can also be formed through selective catalytic reduction. N₂O has historically been considered harmless, and emission regulations for it have been low to non-existent. However, recent attention to global warming and ozone depletion has led to an interest in this gas. N₂O has a global warming potential

310 times that of CO₂, and contributes about 6% of the planet's greenhouse gas emissions [2]. These catalytic converters consist of a honeycomb monolith support [1], which is covered by a thin washcoat containing the active precious metal group (PGM) catalyst. The metals platinum and/or palladium in the DOC are typically used in relatively high loadings compared to the TWC.

A diesel particulate filter (DPF) is placed after the DOC to trap soot, which can be subsequently oxidized by NO₂ produced in the DOC [3]. Another converter, either a selective catalytic reduction unit (SCR) or a lean NO_x trap (LNT) is used to convert NO and NO₂ to nitrogen. Sometimes the DPF and SCR functions are combined [4]. The reduction of NO_x in the SCR depends on the ratio of NO to NO₂, thus the extent of NO oxidation in the DOC is important [5]. Finally, an ammonia slip catalyst may be used to eliminate excess ammonia fed to an SCR [6].

Computer aided design is increasingly being used in the development of catalytic converters. In addition to a good reactor model for the transport equations, such computer simulations require a kinetic model for the reactions. There are two approaches for building kinetic models. The first one is based on the use of mechanistic models [7], which in theory reflect the actual reaction mechanism. The second model type is more empirical, and although may incorporate some mechanistic assumptions, the main concern is to achieve a good correlation of the experimental data. Because all kinetic models require a degree of parameter tuning, all of them thus retain an element of empiricism. The more empirical models are often presented in classical LHHW form. Both approaches have advantages and disadvantages. There is a significant body of

* Corresponding author. Tel.: +1 780 492 3571; fax: +1 780 492 2881.

E-mail address: bob.hayes@ualberta.ca (R.E. Hayes).

literature on global kinetic models for the reactions occurring in a DOC. The work of Voltz et al. [8] is a classical study upon which many of the current empirical models are based. That work dealt with the oxidation of CO and HC in the presence of non-reacting NO. These reactions have been extensively studied and modelled using the Voltz type expression, sometimes with minor modifications [9–12]. This model, and other LHHW style variations on it, has been extended to three-way catalysis with extensive modifications, e.g. Koltsakis et al. [13], as well as diesel oxidation catalysts [14–18].

In this paper, we are interested in a sub-set of the reactions occurring in a DOC. As noted earlier, the primary function of the DOC is to eliminate CO and HC, and to convert some of the NO to NO₂. In the DOC, over a narrow temperature range, some NO can be reduced to nitrogen by the HC, which can be considered to be a desirable reaction. Unfortunately, a partial reduction of NO to N₂O can also occur, as noted earlier. The purpose of this research was to find a global kinetic model for the reactions between NO and HC over Pt and Pt-Pd catalysts. This work was part of a broader effort to develop a comprehensive model for the diesel oxidation catalyst. In a previous paper [12], we presented results for CO and HC alone. In this work, we focus on the reactions and modelling for NO in the presence and absence of HC. The representative HC used in all cases was propene (C₃H₆). The effect of CO will be included in a future publication.

2. Experimental

Experimental data were obtained on Pt and Pt:Pd diesel oxidation catalysts (DOC). The catalysts were provided in the form of a washcoated ceramic monolith with 400 cells per square inch (CPSI). The total precious metal loading was 95 g/ft³ based on total monolith volume. For the bimetallic catalyst, the Pt loading was four times the Pd loading on a mass basis. Catalyst was supplied by Umicore AG. Cylindrical cores of monolith were cut from a full size converter. The cores were 2.29 cm in diameter and 6.10 cm long, to give a total reactor volume of 25 cm³. The catalyst was wrapped in 3 M insulation material, and then inserted into a quartz tube. The tube was placed into a Lindberg Minimite temperature controlled furnace. K-type thermocouples inserted into the monolith channels gave the temperatures at four axial locations, 0 cm, 2 cm, 4 cm and 6 cm from the monolith inlet. Prior to use, the catalyst was aged at 650 °C in flowing air for 16 h.

Each experiment consisted of an ignition extinction (IE) curve. It has been observed in earlier work (and was also seen in this study) that an NO ignition extinction curve shows a hysteresis that is caused by surface oxidation [19,20]. A similar effect has been observed for the oxidation of hydrocarbon and CO mixtures, which could be attributed to a surface coverage by hydrocarbon polymerization products [21]. In this paper we only focus on the light off (ignition) curve. Nevertheless, the reaction rates will be influenced by the reversible deactivation effects. Since in our models the reversible deactivation effects are not explicitly taken into account, these effects will be implicitly included in the determined reaction rates.

In all experiments, the feed stream was introduced to the reactor at temperatures below 80 °C, to avoid reaction before ramping. The temperature was ramped at approximately 3 °C/min. When complete oxidation was achieved, the reactor was cooled by decreasing the furnace temperature to below 80 °C. The base feed stream consisted of 10% O₂, 10% H₂O, 10% CO₂, 300 ppm or 1% He, appropriate reactant gases, with N₂ as the balance. He was added as a tracer to assist with mass spectrometer analysis. Although the mass spec was not used in the experiments reported here, He was always included in the feed. The total gas flow rate was 9.34 L/min

referenced to 298 K and 1 atm pressure. The corresponding space velocity is 20520 h⁻¹ at STP (273 K and 1 atm). The outlet gas composition was measured using a MultiGas 2030 FTIR analyzer (MKS). Before running any experiment, a test with N₂ only (no reactant) was performed to check the temperature difference between the front and the back of the catalyst as well as the radial direction. The test showed that the maximum difference was less than 5 °C between the front and the back and 4 °C in the radial direction (which occurred at high temperature).

During each experiment, temperature and outlet concentration data were obtained every second. This very large data set was reduced in size for the reactor modelling exercise to decrease computational cost. Data points were extracted from the large data set for every delta conversion of the order of 5% or a temperature change of 5 °C, whichever was smaller.

3. Modelling

3.1. Reactor model

To determine the best fit for the kinetic parameters, a reactor model is necessary. For this work, the main requirement is for a fast execution speed, because of the number of simulations that must be performed. Therefore, we used a one dimensional pseudo-homogeneous steady state plug flow single channel model (SCM). The use of the SCM implies that all channels in the monolith have the same conditions. Only the appropriate mass conservation equations are solved, and not the energy balance. The reactor temperature measured at each time step was imposed in the model, with linear interpolation used for the points between the measured values. It is not possible to include the energy balance, because the reactor is not adiabatic and the rates of heat transfer to and from the reactor are not known. Since the temperature along the centre line of the reactor is known at four locations, the simulator uses these four temperatures to impose a temperature profile along the reactor.

Even though the experiments are transient, it is acceptable to use a steady state model. The residence time in the reactor is very small, of the order of 0.02 s. The temperature change of the solid is much slower, so in effect the gas is always in a pseudo-steady state with the wall temperature. Because the temperature is measured, the steady state model will give a good solution. The ignition curve was constructed by performing a sequence of steady state simulations with increasing reactor temperatures, based on the experimental values.

The mole balance equation is written for each species of interest. For species *j* we have:

$$-Cu_m \frac{dY_j}{dz} - (-R_j) \frac{V_W}{V_C} = 0 \quad (1)$$

The mean velocity in the channel is denoted *u_m* and the bulk molar concentration of the gas is *C*, which is computed from the ideal gas law. The reaction rate for a catalytic converter is usually based on the washcoat volume, and therefore it must be converted to a basis of channel volume for the homogeneous model. Thus the ratio of washcoat volume (*V_W*) and the channel volume (*V_C*) are included to provide the correct basis for the reaction rate. If we assume that the channel can be represented as a right circular cylinder of a length of *z*, diameter *D_H*, and that the washcoat occupies an annular ring of outside diameter *D_{WC}*, then with the appropriate substitution, we obtain:

$$-Cu_m \frac{dY_j}{dz} - (-R_j)_V \frac{(D_{WC}^2 - D_H^2)}{D_H^2} = 0 \quad (2)$$

The equation can be explicitly arranged to give:

$$-\frac{dY_j}{dz} = \frac{(-R_j)_V}{Cu_m} \frac{(D_{WC}^2 - D_H^2)}{D_H^2} \quad (3)$$

The resulting kinetic parameters are therefore global, in that they include all heat and mass transfer effects implicitly, and are not necessarily intrinsic rate constants. Substitution of all constants into the mole balance equation gives:

$$-\frac{dY_j}{dz} = 7.688 \times 10^{-3} (-R_j)_V \quad (4)$$

The software MATLAB was used to solve the differential equations simultaneously. Because computation time was important and the equations are quite stiff, the NAG toolbox solver, "d02ej" was used. This solver is almost two times faster than regular MATLAB solvers (e.g. ode15s or ode45).

3.2. Parameter estimation

An optimization procedure is required to minimize the objective function. Sola et al. [12] used a General Pattern Search (GPS) algorithm. The GPS is a gradient free method, thus computation of the gradients is not necessary [22]. This method can be easily coupled to "black box" solvers. In the case where the solver returns an invalid result e.g. division by zero, the optimizer can simply discard the result and continue without halting. Although GPS is a very powerful algorithm for finding a global minimum, it has some drawbacks for this problem. There are more than 16 parameters in some of the models tested, and the potential range of the parameters is quite wide. This made the use of the GPS rather time consuming. As an alternative, a combination of two optimizers was used.

The MATLAB algorithm fmincon was used as the main optimization tool. This gradient based algorithm attempts to find a constrained minimum of a scalar multivariable function starting at an initial point. The main drawback is that a good initial guess is required; otherwise the method can become trapped in a local minimum. Therefore, providing a reasonable initial point for fmincon can significantly increase the accuracy of the results. A genetic algorithm (GA) was used as a preliminary optimizer to locate reasonable initial points to start fmincon.

The GA is a non-gradient method which can be used for solving both constrained and unconstrained problems. Basically, it works based on biological evolution theory. At each step, GA uses a pair of current population as parents to produce children for next generation. Over successive generations, the population evolves towards an optimal solution. We used GA to scan a wide parameter range to find the best initial value for fmincon. Combining these two methods gave better results in comparison with GPS algorithm.

The objective function was defined in terms of the fractional conversion of a reactant into a designated product. The general formula for species j can be written:

$$O_i = \frac{1}{n} \sum_{i=1}^n (X_{\text{exp}} - X_{\text{pred}})^2 \quad (5)$$

As we discussed before, we use LHHW type models. These models contain kinetic and adsorption parameters in the Arrhenius form. Is an aid in optimization, these parameters were written in the following form:

$$k_i = \exp \left(A_i - \frac{E_i}{R_g} \left[\frac{1}{T} - \frac{1}{450} \right] \right) \quad (6)$$

$$K_i = \exp \left(B_i - \frac{H_i}{R_g} \left[\frac{1}{T} - \frac{1}{450} \right] \right) \quad (7)$$

The temperature of 450 K was used in the exponential, being in the centre of the ignition curves for the experimental range of conditions considered.

4. Modelling the oxidation of NO

Although the primary goal was to model the combined reactions of NO and C₃H₆, in the first instance we consider the oxidation of NO only, that is, without the presence of propene. The overall reaction can be expressed as:



There is a lot of work reported in the literature that deals with the oxidation of NO on platinum catalyst. A feature of this reaction is that it is equilibrium limited at higher temperatures. The key global models presented in the literature are reviewed by Hauptmann et al. [23], and the main ones that have been reported are summarized in the following. We tested five models during the course of this investigation. The first model (Model 1) presented is based on a form used by Sampara et al. [18] and Pandya et al. [14]. This model accounts for self-inhibition by NO, but inhibition by NO₂ is not considered:

$$(-R_{NO}) = \frac{k_4 Y_{NO} Y_{O_2}^{0.5}}{(1 + K_8 Y_{NO})} (1 - \beta) \quad (9)$$

The equilibrium term is:

$$\beta = \left[\frac{1}{K_{eq}} \frac{1}{\sqrt{P}} \frac{Y_{NO_2}}{Y_{NO} (Y_{O_2})^{0.5}} \right] \quad (10)$$

The pressure, P , has units of bar. Most papers do not include the pressure in their equilibrium term; however, most investigations are carried out at or near one bar pressure. The equilibrium constant as a function of temperature is given by:

$$K_{eq} = \exp \left(5.045 + \frac{6.344 \times 10^3}{T} - 2.3 \ln(T) + 3.031 \times 10^{-3} T - 8.281 \times 10^{-7} T^2 + 1.142 \times 10^{-10} T^3 \right) \quad (11)$$

Our Model 2 is the equation proposed by Mulla et al. [24,25], who developed a model that included NO₂ inhibition. They stated that it was consistent with experimental data.

$$(-R_{NO}) = \frac{k_4 Y_{O_2}}{(1 + K_8(Y_{NO_2}/Y_{NO}))} (1 - \beta) \quad (12)$$

Model 3 is the expression reported by Bhatia et al. [26], which also includes inhibition by NO₂:

$$(-R_{NO}) = \frac{k_4 Y_{O_2}^{0.5}}{(1 + K_8 Y_{NO} + K_{10}(Y_{NO_2}/Y_{NO}))} (1 - \beta^2) \quad (13)$$

In this work, we also use this model in slightly modified form, which we call Model 4, with the equilibrium expression raised to the power one, in keeping with common practice.

$$(-R_{NO}) = \frac{k_4 Y_{O_2}^{0.5}}{(1 + K_8 Y_{NO} + K_{10}(Y_{NO_2}/Y_{NO}))} (1 - \beta) \quad (14)$$

Model 5 is the one proposed by Hauff et al. [15] as part of a general model for a diesel oxidation catalyst (DOC):

$$(-R_{NO}) = \frac{k_4 Y_{NO} Y_{O_2}^{0.5}}{(1 + K_8 Y_{NO} + K_{10} Y_{NO_2})^2} (1 - \beta) \quad (15)$$

We remark at this point that in the form of the Voltz model and its derivative versions commonly employed in the literature,

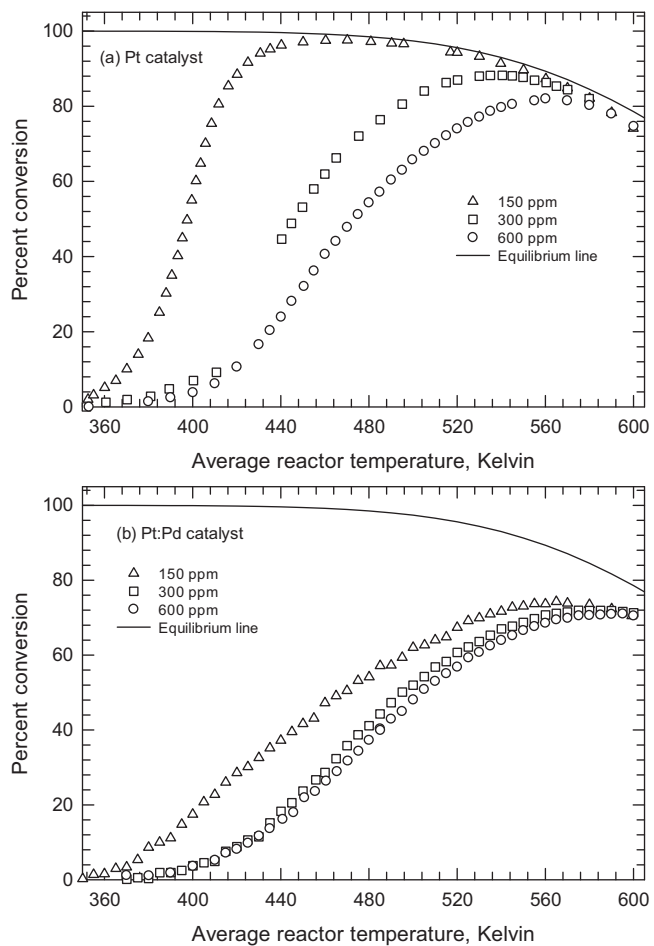


Fig. 1. Experimental ignition curves for the NO oxidation on (a) Pt catalyst and (b) Pt:Pd bimetallic catalyst.

a temperature term appears in the denominator. This term was introduced by Oh and Cavendish [10]. In Sola et al. [12], it was observed that the presence or absence of this term made no significant difference in the closeness of fit in the models for CO and C₃H₆ oxidation. In the current work, we tested all of our proposed models (both for NO and C₃H₆ oxidation) with and without a *T* term, and again found only a small difference in the result, in terms of the minimum residuals obtained (although obviously with different model parameter values). We have therefore decided not to include this term, and all further discussion will relate to the model without *T* in the denominator. The Models 1 to 5 contain up to six adjustable parameters.

For this set of experiments, the only product is NO₂, thus there is a single reaction, and a single objective function, based on the fractional conversion of NO.

$$O_{NO} = \frac{1}{n} \sum_{i=1}^n [(X_{NO})_{pred} - (X_{NO})_{exp}]^2 \quad (16)$$

Each ignition curve (that is each experiment) produces one objective function. For each catalyst, three inlet concentrations of NO were used with the basic feed composition described earlier. The three nominal concentrations were 150, 300 and 600 ppm of NO. The ignition curves obtained for the two catalysts are shown in Fig. 1. The overall objective function that was minimized for each catalyst is the sum of the three ignition curves thus produced.

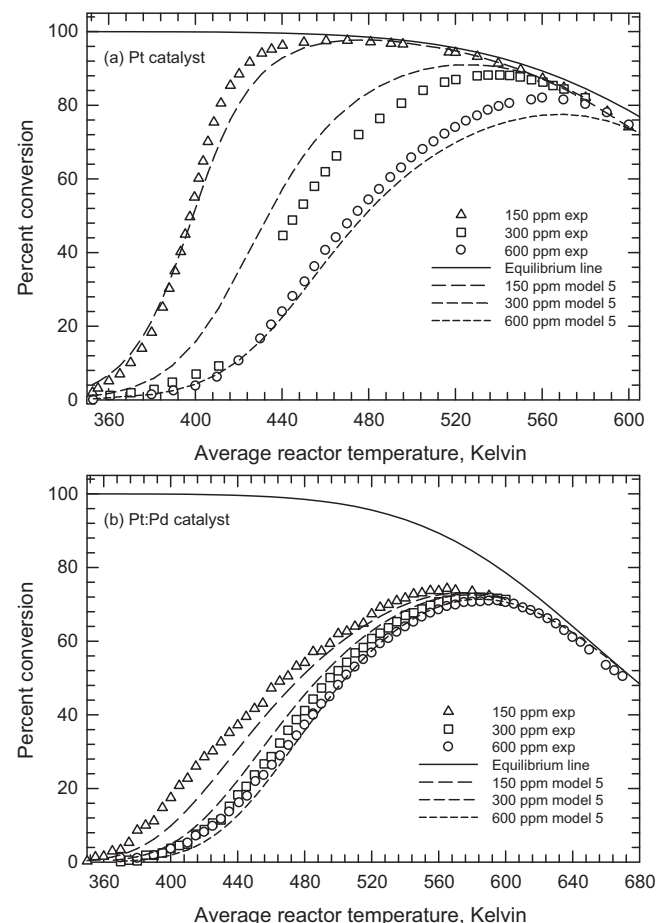


Fig. 2. Simulation results from Model 5 and experimental ignition curves for the NO oxidation on (a) Pt catalyst and (b) Pt:Pd bimetallic catalyst. In each case, three experiments were used in the optimization procedure. The symbols represent experimental values and the lines the simulation results.

In other words, the three experiments for each catalyst were fit simultaneously to the models.

We observe from the results a self-inhibition of the oxidation reaction by the reactant NO. Also, it is seen that the Pt catalyst is more active than the bimetallic Pt:Pd one. The limitation of conversion by equilibrium is also evident.

The five models were tested for their ability to fit the experimental data. As previously seen, when fitting the parameters in the CO and HC models [12], it was relatively easy to obtain a very good fit for any of the models when fitting the ignition curve for a single experiment. However, if this is done, there is a wide difference in the parameter values for each experiment, and thus to validate the models it was essential to use all three curves together.

The models that fit the data well varied for the two catalysts. For the Pt catalyst, Models 3, 4 and 5 gave a reasonable fit, whilst Models 1 and 2 were quite far from acceptable, with Model 2 being the worst. For the bi-metallic Pt:Pd catalyst, Models 1 and 5 gave a good result, virtually the same degree of fit, with the other models being unacceptable. Model 5 was thus the only model that is able to correlate the data for both catalysts. The results of the Model 5 simulations are shown in Fig. 2 for both catalysts. The parameter values are given in Table 1. In all cases where parameter values are given the activation energies and heats of adsorption have units of J/mol, and the reaction rates have units of mol/(m³ s), where the volume refers to the washcoat volume.

Table 1

Parameter values for Model 5 for the NO oxidation curves. The activation energies and heats of adsorption have units of J/mol, and the reaction rates have units of mol/(m³ s), where the volume refers to the washcoat volume.

Parameter	Pt catalyst	Pt:Pd catalyst
k_4	A_4	29.6
	E_4	1074
K_8	B_8	18.2
	H_8	-34 692
K_{10}	B_{10}	18.7
	H_{10}	-13 626
		8.43
		15 667
		7.27
		-43 455
		7.32
		-49 463

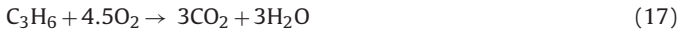
Table 2

Parameter values for the C₃H₆ oxidation curves. The activation energies and heats of adsorption have units of J/mol, and the reaction rates have units of mol/(m³ s), where the volume refers to the washcoat volume.

Parameter	Pt catalyst	Pt:Pd catalyst
k_3	A_3	26.20
	E_3	26 444
K_6	B_6	15.1
	H_6	-21 646
		13.3
		44 176
		7.13
		-32 150

5. Modelling the oxidation of propene

The oxidation of propene has been widely modelled in the literature, usually as part of a programme that includes CO. The oxidation reaction is:



In the context of catalytic converters, the most common model for this oxidation reaction is the one presented by Voltz et al. [8], which is:

$$(-R_{\text{C}_3\text{H}_6}) = \frac{k_3 Y_{\text{C}_3\text{H}_6} Y_{\text{O}_2}}{(1 + K_6 Y_{\text{C}_3\text{H}_6})^2} \quad (18)$$

It was previously shown that this model was adequate for the Pt catalyst [12]. For an excess of oxygen, and in the absence of CO and NO, this model is essentially the same as used more recently by Hauff et al. [15] in their global model of the DOC.

For both catalysts, we used three ignition curves at nominal propene concentrations of 250, 500 and 750 ppm by volume. All three curves were used in the optimization process to obtain the best fit model parameters, in the same manner as was done for the NO oxidation curves. The objective function for an ignition curve is:

$$O_{\text{C}_3\text{H}_6} = \frac{1}{n} \sum_{i=1}^n [(X_{\text{C}_3\text{H}_6})_{\text{pred}} - (X_{\text{C}_3\text{H}_6})_{\text{exp}}]^2 \quad (19)$$

The results obtained for both experiment and model are shown in Fig. 3 for the two catalysts. The model parameter values are given in Table 2. It is seen in both cases that the fit of the model is quite good. Also, the self-inhibition of the reaction by propene is also observed, consistent with literature results.

6. Modelling the combined system

We consider now the combined reaction system with propene and NO in the feed. In addition to the oxidation reactions of NO and of C₃H₆, over a small temperature range, some NO will be reduced by C₃H₆. This reaction is called selective catalytic reduction (SCR). The SCR of NO by hydrocarbons has been extensively reported in the literature over a variety of catalysts since the reaction was first reported in 1990 [27,28]. A good early review of the process is given in Amiridis et al. [29]. As seen in this review, as well as other literature, there have been several catalysts suggested for

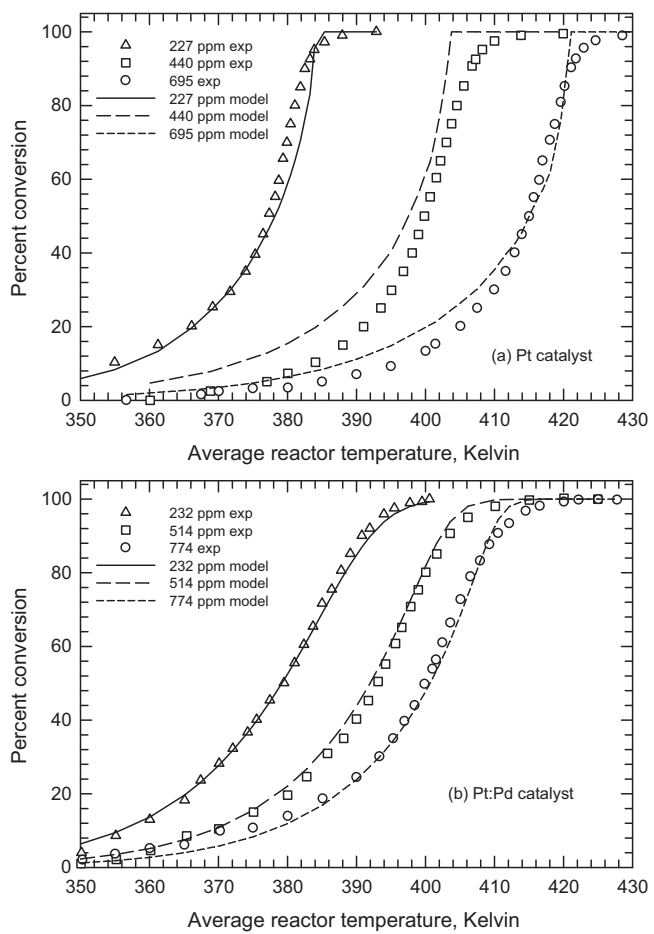
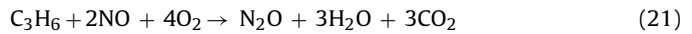
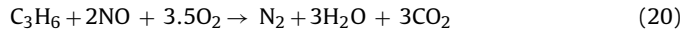


Fig. 3. Simulation results and experimental ignition curves for the C₃H₆ oxidation on (a) Pt catalyst and (b) Pt:Pd bimetallic catalyst. In each case, three experiments were used in the optimization procedure. The symbols represent experimental values and the lines the simulation results.

the reaction; however, in this work we will only discuss Pt based systems. Initial discussion centred on the possible use of hydrocarbon based SCR as a means of controlling NO_x emissions from a diesel engine, although the drawbacks of this method have prevented its widespread adoption. Nevertheless, some SCR of NO by hydrocarbons is present in a DOC, and therefore the reactions must be included in any comprehensive model for a DOC. In addition, the partial reduction of some NO to N₂O may also occur, which is an undesirable reaction because N₂O is a strong greenhouse gas, and also leads to formation of NO in the upper atmosphere [2]. It has been observed that the SCR of NO depends to an extent on the hydrocarbon present [30–32], and that N₂O production is also affected by the hydrocarbon present [33]. Over a PGM catalyst, SCR can be represented by the following global reactions:



We can also potentially have the reaction between NO₂ and propene to form NO:

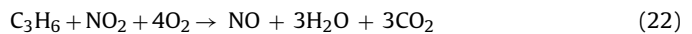


Table 3

NO and propene experiments, inlet concentrations. The concentrations have units of ppm on a volume (molar) basis.

Run	Catalyst type	Propene, ppm	NO, ppm
13	Pt	500	150
14	Pt	500	300
15	Pt	500	600
16	Pt:Pd	500	150
17	Pt:Pd	500	300
18	Pt:Pd	500	600
20	Pt:Pd	750	300
21	Pt:Pd	750	600

Because the NO that reacts produces NO_2 , N_2 and N_2O , we have to define fractional conversions on this basis. Thus, we define (a) the conversion of NO to NO_2 as:

$$X_{\text{NO}_2} = \frac{(Y_{\text{NO}_2})_f}{(Y_{\text{NO}})_0} \quad (23)$$

(b) The conversion of NO to N_2O as:

$$X_{\text{N}_2\text{O}} = \frac{2(Y_{\text{N}_2\text{O}})_f}{(Y_{\text{NO}})_0} \quad (24)$$

(c) The conversion of NO to N_2 (that is, NO_x conversion) as:

$$X_{\text{NO}_x} = \frac{(Y_{\text{NO}})_0 - [(Y_{\text{NO}})_f + 2(Y_{\text{N}_2\text{O}})_f + (Y_{\text{NO}_2})_f]}{(Y_{\text{NO}})_0} \quad (25)$$

The fractional conversion of propene is computed based on inlet and outlet mole fraction, in the usual way. For each experiment, we can then define four objective functions:

$$O_{\text{C}_3\text{H}_6} = \frac{1}{n} \sum_{i=1}^n [(X_{\text{C}_3\text{H}_6})_{\text{pred}} - (X_{\text{C}_3\text{H}_6})_{\text{exp}}]^2 \quad (26)$$

$$O_{\text{NO}_2} = \frac{1}{n} \sum_{i=1}^n [(X_{\text{NO}_2})_{\text{pred}} - (X_{\text{NO}_2})_{\text{exp}}]^2 \quad (27)$$

$$O_{\text{N}_2\text{O}} = \frac{1}{n} \sum_{i=1}^n [(X_{\text{N}_2\text{O}})_{\text{pred}} - (X_{\text{N}_2\text{O}})_{\text{exp}}]^2 \quad (28)$$

$$O_{\text{NO}_x} = \frac{1}{n} \sum_{i=1}^n [(X_{\text{NO}_x})_{\text{pred}} - (X_{\text{NO}_x})_{\text{exp}}]^2 \quad (29)$$

The total objective function is the sum of these four functions, and the objective function to be minimized is the sum of the total objective functions for all experiments with mixed feed for each of the two catalysts.

$$O_{\text{Total}} = O_{\text{C}_3\text{H}_6} + O_{\text{NO}_2} + O_{\text{N}_2\text{O}} + O_{\text{NO}_x} \quad (30)$$

There were three experiments for the Pt catalyst and five for the Pt:Pd catalyst. The concentrations of NO and C_3H_6 are given in Table 3 for these runs. Note that the run numbers are the same as used by Sola-Quiroz [16] for the Pt catalyst and Khosravi-Hafshejani [17] for the Pt:Pd catalyst. A typical response at the reactor outlet is given in Fig. 4, which represents experiment number 16. The following observations can be made about the results obtained:

- (1) The SCR of NO starts shortly after the ignition of propene commences. This behaviour has been reported by Ansell et al. [34]. In their study, they concluded based on a temporal analysis of products (TAP) that the rate of NO reduction depends on the rate of reduction of the platinum surface, which is in turn caused by

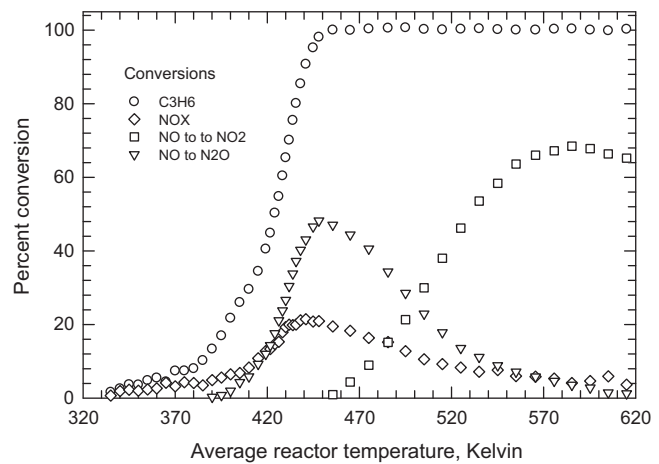


Fig. 4. Typical experimental ignition curves for an experiment with both C_3H_6 and NO in the feed. Experiment number 16.

the propene oxidation. Thus the rates of propene oxidation and NO reduction are coupled.

- (2) There is a preferential production of N_2O compared to N_2 .
- (3) Oxidation of NO to NO_2 starts after the rate of SCR has peaked and starts to decline. This point occurs when the fractional conversion of C_3H_6 reaches 100%.

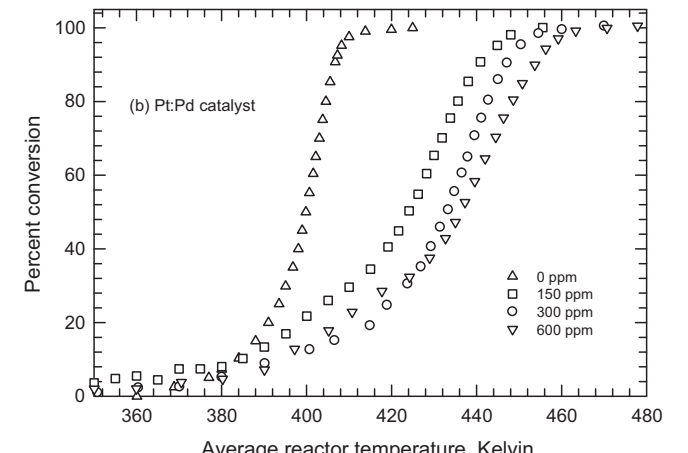
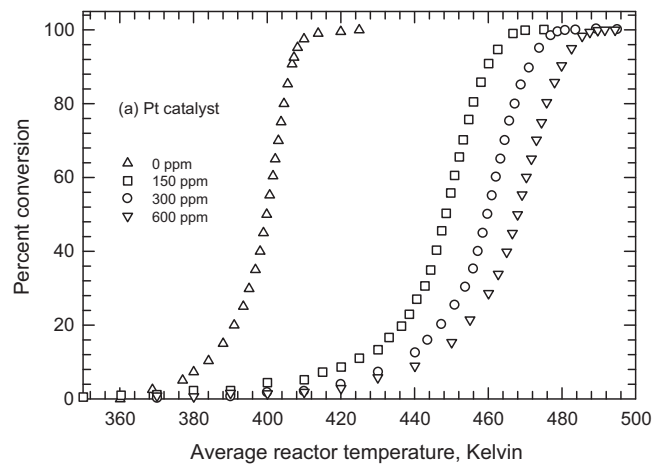


Fig. 5. Experimental ignition curves for the C_3H_6 oxidation on (a) Pt catalyst and (b) Pt:Pd bimetallic catalyst with increasing concentrations of NO. The NO inhibits the propene ignition.

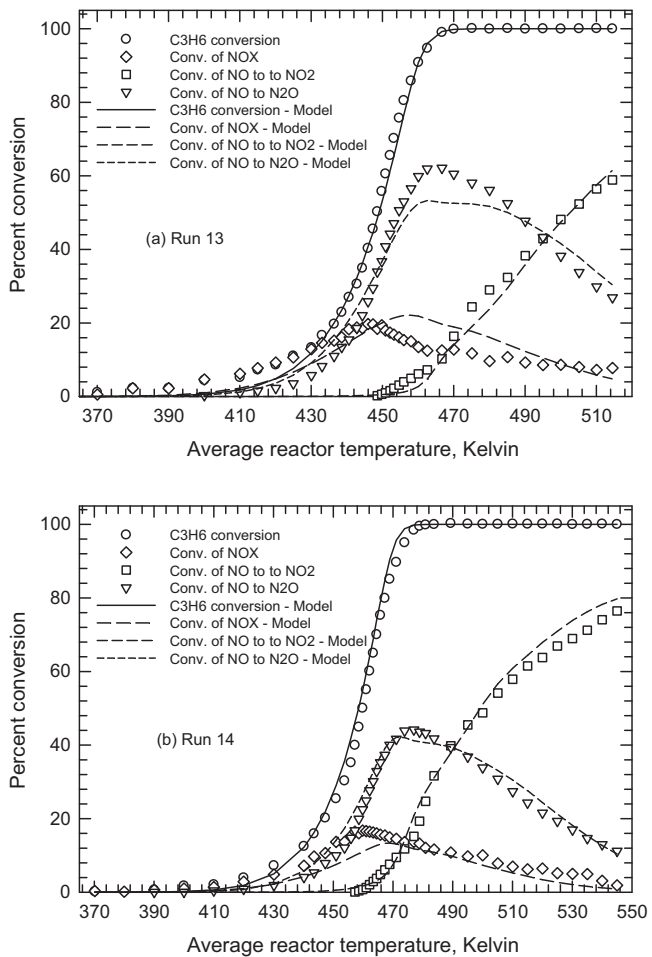


Fig. 6. Typical experimental and model ignition curves for the mixed feed experiments on Pt catalyst: (a) Run 13 and (b) Run 14. The symbols represent experimental values and the lines the simulation results.

- (4) The maximum conversion by SCR occurs near the point where the fractional conversion of propene at the reactor outlet increases to near 100%, which is consistent with the literature [35].
- (5) For a constant HC concentration, the fraction of the NO reduced declines as the NO concentration increases.
- (6) For a constant NO concentration, an increase in the HC concentration increases the fractional conversion of NO by SCR. The selectivity is relatively unchanged.

In addition to these points listed above, it is also observed that the presence of NO inhibits the ignition of C₃H₆, which is in agreement with the results of Burch and Millington [36]. Fig. 5 shows the propene ignition curves obtained for a nominal 500 ppm propene with increasing levels of NO in the feed. The same trend was observed for both catalysts. As noted in the comments presented above, the presence of propene delays the oxidation of NO to NO₂. Indeed, as noted, the oxidation of NO to NO₂ appears not to occur when there is a measurable concentration of C₃H₆. Alternatively, if NO₂ is produced, it is possible that it is quickly reduced to NO by the presence of C₃H₆.

To build the models for testing, all of this observed behaviour must be accounted for. As far as possible, we build our models based on the current state of the literature. There are a few models for propene oxidation in the presence of NO reported in the literature.

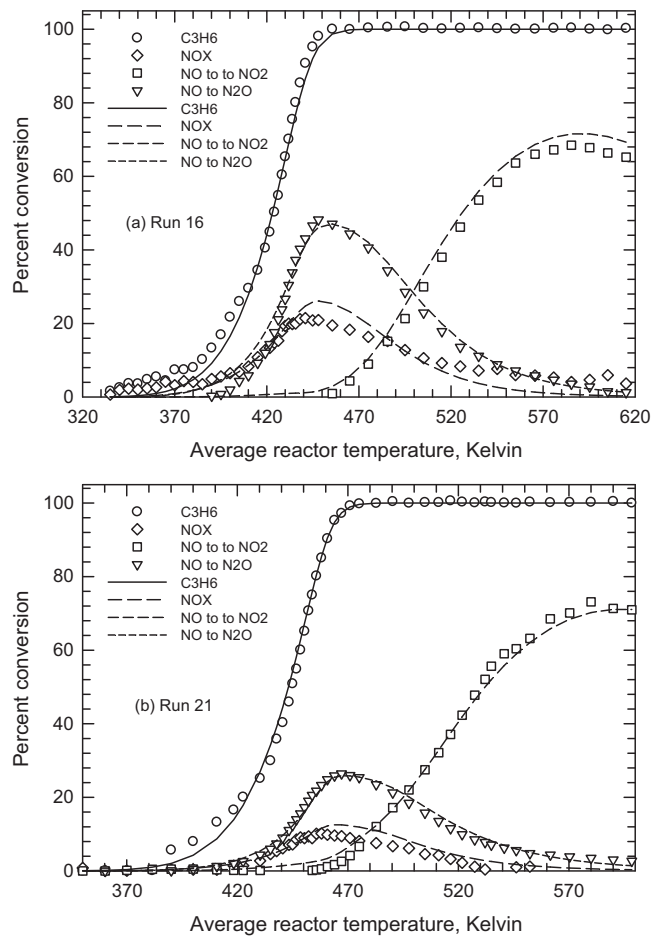


Fig. 7. Typical experimental and model ignition curves for the mixed feed experiments on Pt:Pd catalyst: (a) Run 16 and (b) Run 21. The symbols represent experimental values and the lines the simulation results.

The most common and classical is the model of Voltz et al. [8]. In the form as modified by Sola et al. [12] the equation is:

$$(-R_{C_3H_6}) = \frac{k_3 Y_{C_3H_6} Y_{O_2}}{(1 + K_6 Y_{C_3H_6})^2 (1 + K_8 Y_{NO})} \quad (31)$$

In the work of Voltz the NO was considered as an adsorbing but non-reacting species. Hauff et al. [15] included the inhibition term for NO in a common denominator.

$$(-R_{C_3H_6}) = \frac{k_3 Y_{C_3H_6} Y_{O_2}}{(1 + K_6 Y_{C_3H_6} + K_8 Y_{NO})^2} \quad (32)$$

We also mention the model used by Ansell et al. [34], which is similar to the Voltz model, except that the power of the inhibition term (denominator) was 1 rather than 2. We did not find that this model was successful for fitting the C₃H₆ oxidation curves, and thus this model was not considered further.

We can couple the HC oxidation model with a model for the oxidation of NO. There are two approaches that can be taken in this regard. In the first approach we consider only experiments in which both HC and NO are present. This approach leads to certain model forms. As noted in the comments, the oxidation reaction of NO to NO₂ does not appear to proceed until the conversion of HC is 100%. When the reactor temperature reaches the point where 100% conversion is first attained, it is clear that this occurs at the reactor exit. As the reactor temperature increases further, the 100% conversion point moves upstream towards the reactor inlet. It is then postulated that only in the reactor length where there is negligible HC

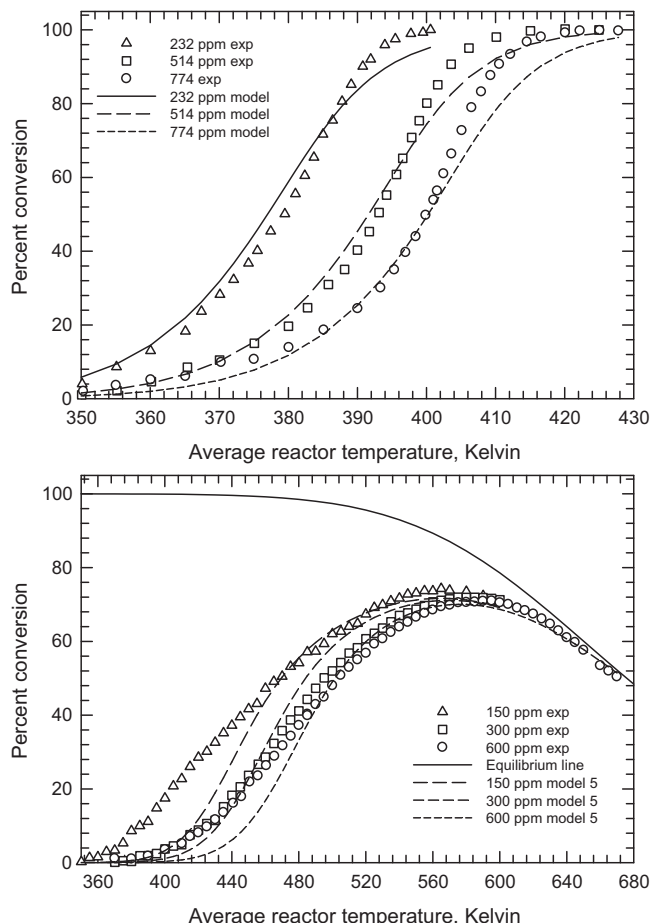


Fig. 8. Experimental and model ignition curves for the single feed and mixed feed experiments on Pt:Pd catalyst. Optimization performed using all nine experiments. (a) Propene ignition and (b) NO ignition. The symbols represent experimental values and the lines the simulation results.

will net NO oxidation occur. Therefore, from a purely fitting standpoint, and provided that we consider only experiments with mixed feed, then the concentration of C_3H_6 does not need to appear in the NO oxidation sub-model. Thus we can consider five models for NO oxidation as given by Eqs. (16)–(20). We stress that the overall model thus found would not work for a system without C_3H_6 , because there is then nothing in the sub-model to allow for the delayed breakthrough of the NO oxidation curve. We observe that in their DOC model, Hauff et al. [15] did not have a C_3H_6 inhibition term in their NO oxidation equation.

In the second approach to developing a model, we try to find a system that will reproduce experiments with mixed feed, as well as those with only NO or C_3H_6 only. This second approach is discussed later.

A good starting point for discussion is the model proposed by Ansell et al. [34], who coupled the rate of NO reduction to the rate of oxidation of propene:

$$(-R_{NO})_{r1} = (-R_{C_3H_6}) \frac{k_2 Y_{NO}}{(1 + K_9 Y_{O_2})(1 + ZY_{NO})} \quad (33)$$

They observed that to account for the sharp decline in NO reduction at higher temperature, it was necessary to add an inhibition term for oxygen that increased with temperature. This term was mechanistically justified as representing a competitive adsorption between NO and oxygen. Ansell did not present theoretical justification for including the temperature independent NO inhibition term in the denominator, although it fit their data well.

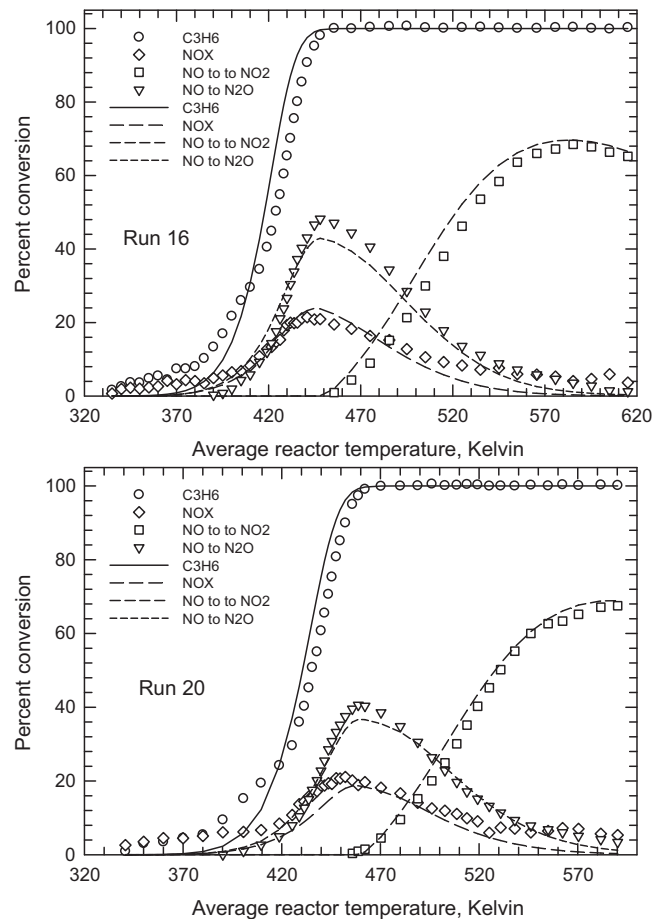


Fig. 9. Experimental and model ignition curves for the single feed and mixed feed experiments on Pt:Pd catalyst. Optimization performed using all nine experiments. (a) Run 16 and (b) Run 21. The symbols represent experimental values and the lines the simulation results.

Pandya et al. [14] used a simpler version of Eq. (33) as part of a DOC model on a Pt catalyst, viz.:

$$(-R_{NO})_{r1} = (-R_{C_3H_6}) \frac{k_2 Y_{NO}}{(1 + K_9 Y_{O_2})} \quad (34)$$

They reported a good agreement with a smaller sample of experimental results. We note here without further discussion Eq. (34) was tested during the course of this investigation, and the results were not satisfactory.

Many efforts have been made to understand the mechanism of NO reduction by hydrocarbons. The reaction mechanism is strongly affected by reaction conditions such as gas composition, temperature and type of hydrocarbon [37–39]. Burch et al. [40–42] proposed a dissociative mechanism for Pt catalyst. In this reaction, the NO undergoes dissociative adsorption to N and O. The adsorbed O reacts with propene or its adsorbed fragments to form CO₂ and H₂O. The adsorbed N reacts to form N₂ or with an NO molecule to form N₂O. Alternative mechanisms that proceed via more complex organic intermediates have also been proposed [40].

Burch and Millington [36] showed that even with high presence of oxygen in lean condition, oxygen coverage on the Pt surface is small, while C_3H_6 coverage on catalyst site is at saturation. The double bond of propene make it possible to react strongly with Pt sites which results a high coverage of propene on the surface [35]. So there is no active site available for NO to react until adsorbed hydrocarbon species react, which means reduction of NO is secondary and dependent on reduction of the active sites by propene oxidation.

Table 4

Parameter values for the SCR model based on experiments with mixed feed only. Parameters for Eqs. (32), (35), (37) and (39). The activation energies and heats of adsorption have units of J/mol, and the reaction rates have units of mol/(m³ s), where the volume refers to the washcoat volume.

Parameter	Pt catalyst	Pt:Pd catalyst
k_2	A_2	16.2
	E_2	77 641
k_3	A_3	15.0
	E_3	20 619
k_4	A_4	11.3
	E_4	149 475
k_{11}	A_{11}	16.7
	E_4	118 548
K_6	B_6	9.91
	H_6	-6415
K_8	B_8	11.1
	H_8	-87 226
K_9	B_9	10.1
	H_9	149 916
K_{10}	B_{10}	15.0
	H_{10}	-103 226
K_{12}	B_{12}	7.00
	H_{12}	-0.0242
K_{13}	B_{13}	8.64
	H_{13}	-318
		-82 979

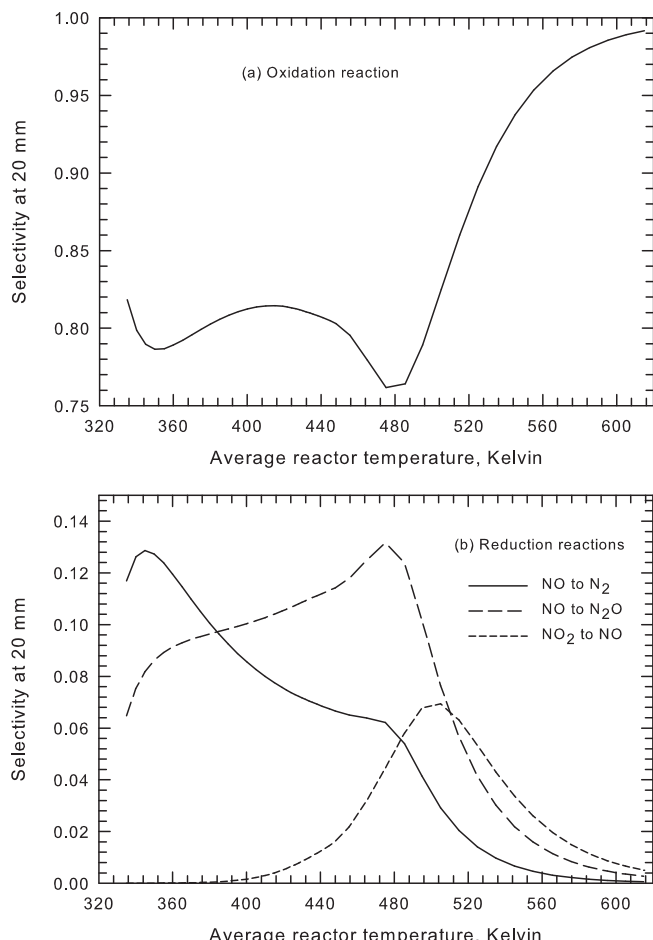


Fig. 10. Local selectivity for the reaction of propene in the oxidation and reduction reactions. The values correspond to a position 20 mm from the reactor inlet. (a) Oxidation of propene and (b) reduction reactions for NO_x.

On the other hand, after reduction of the catalyst surface by hydrocarbon oxidation, NO will adsorb on the surface and will be reduced to N₂ or N₂O. After the decomposition of NO, adsorbed oxygen will build up on the catalyst surface, oxidizing it. This effect can be interpreted as self-poisoning by NO, because oxidized sites cannot adsorb and decompose further NO molecules [39].

These two effects, hydrocarbon inhibition effect on NO reduction and NO self-poisoning effect, should be considered to have a realistic model. Based on these observations, the rate of oxidation of propene should be coupled to the rate of reduction of NO, and should contain NO and possibly HC inhibition terms.

Following from the above discussion, Khosravi-Hafshejani [17] added an inhibition term to the reduction rate equations for the propene, to give the following model:

$$(-R_{NO})_{r1} = (-R_{C_3H_6}) \frac{k_2 Y_{NO}}{(1 + K_9 Y_{O_2})(1 + K_{12} Y_{NO})(1 + K_{13} Y_{C_3H_6})} \quad (35)$$

If we assume that the route to N₂O proceeds along the same lines as for N₂, then by analogy we can write a model for the reduction of NO to N₂O as:

$$(-R_{NO})_{r2} = (-R_{C_3H_6}) \frac{k_{11} Y_{NO}}{(1 + K_9 Y_{O_2})(1 + K_{12} Y_{NO})} \quad (36)$$

Including the additional hydrocarbon inhibition term gives:

$$(-R_{NO})_{r2} = (-R_{C_3H_6}) \frac{k_{11} Y_{NO}}{(1 + K_9 Y_{O_2})(1 + K_{12} Y_{NO})(1 + K_{13} Y_{C_3H_6})} \quad (37)$$

We also allow for the reduction of NO₂ (if formed) back to NO by hydrocarbon. Because this reaction is fast, the rate constant was set to be ten times higher than the rate constant for NO reduction, thus, the following two variations exist:

$$(-R_{NO_2}) = (-R_{C_3H_6}) \frac{10k_2 Y_{NO_2}}{(1 + K_9 Y_{O_2})(1 + K_{12} Y_{NO})} \quad (38)$$

$$(-R_{NO_2}) = (-R_{C_3H_6}) \frac{10k_2 Y_{NO_2}}{(1 + K_9 Y_{O_2})(1 + K_{12} Y_{NO})(1 + K_{13} Y_{C_3H_6})} \quad (39)$$

To summarize, and considering the model development discussed in the foregoing, we see that we have two possible models for the oxidation of C₃H₆ and five for the oxidation of NO. For

Table 5

Parameter values for the SCR model based on experiments with single feed (HC or NO) and mixed feed. Parameters for Eqs. (32), (35), (37)(39) and (40). The activation energies and heats of adsorption have units of J/mol, and the reaction rates have units of mol/(m³ s), where the volume refers to the washcoat volume.

Parameter	Pt:Pd catalyst	
k_2	A_2	22.0
	E_2	6865
k_3	A_3	12.1
	E_3	20 000
k_4	A_4	8.73
	E_4	9404
k_{11}	A_{11}	22.6
	E_4	19 493
k_6	B_6	6.15
	H_6	-50 240
k_8	B_8	8.06
	H_8	-56 873
K_9	B_9	14.0
	H_9	140 362
K_{10}	B_{10}	6.30
	H_{10}	-51 338
K_{12}	B_{12}	3.92
	H_{12}	-0.107
K_{13}	B_{13}	12.4
	H_{13}	-103 566
K_{14}	B_{14}	14.9
	H_{14}	-146 662

the reduction reaction subset, we have two possibilities. We thus have a possible model set of twenty combinations. Space limitations prevent the presentation of all of the results graphically; therefore we will describe the results and present the experimental and model comparisons for the models which worked the best only.

We consider first the oxidation reactions. We observed that both of the hydrocarbon oxidation models worked essentially equally well. There was no discernible difference visually between the graphs produced. For the platinum catalyst, all of the NO oxidation models gave essentially the same fit as well. This was in contrast to the experiments run with NO alone, in which models 1 and 2 did not give good results. For the Pt:Pd catalyst, only oxidation models 1 and 5 gave a good reproduction of the NO oxidation curve, which was also the case for the experiments when only NO was used.

For the reduction reactions, for the Pt catalyst, the fit was the same for both models; that is with and without the extra hydrocarbon inhibition term. For the Pt:Pd catalyst, the fit for some of the runs was acceptable without the extra hydrocarbon inhibition term. With the addition of the HC inhibition term, the fit was much better and acceptable for all experiments. If

all of the experiments performed are considered, then we suggest that model 5 for the NO oxidation coupled with the C_3H_6 oxidation model recommended by Hauff et al. [15] would be the best one, with the most general applicability. We present now some results using this model, that is, using Eqs. (15), (32), (35), (37) and (39). The parameter values for this model for the two catalysts are given in Table 4.

Fig. 6 shows the results from this model for Runs 13 and 14 (Pt catalyst), whilst Fig. 7 shows the results for Experiments 16 and 21 (Pt:Pd catalyst). The fit is apparently quite good, and this is the typical level of fit achieved with this model.

We discussed early that we can attempt to find a model that will fit not only the mixed feed runs, but also the NO oxidation alone and the C_3H_6 oxidation alone runs. We performed this optimization for the Pt:Pd catalyst, using the 3 HC oxidation curves, the 3 NO oxidation curves, and the five runs with mixed feed. As noted earlier, the form of the NO oxidation model used to date will obviously not work in this case, because there is no term to allow for the delay in the onset of the NO oxidation when C_3H_6 is present. We therefore introduce another hydrocarbon inhibition term into the NO oxidation expression:

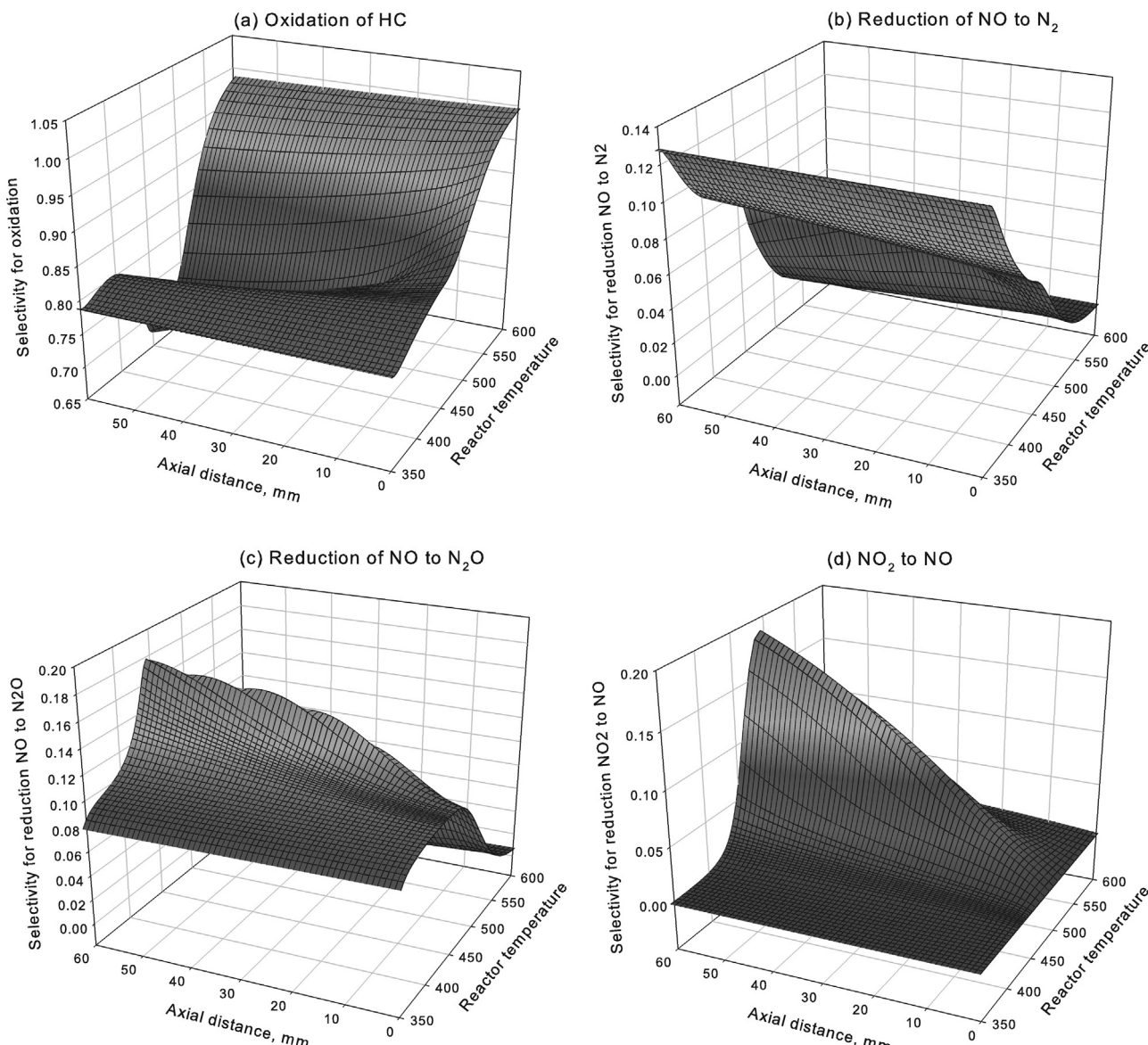


Fig. 11. Local selectivity for the reaction of propene in the oxidation and reduction reactions.

$$(-R_{NO}) = \frac{k_4 Y_{NO} Y_{O_2}^{0.5}}{(1 + K_{14} Y_{C_3H_6} + K_8 Y_{NO} + K_{10} Y_{NO_2})^2} (1 - \beta) \quad (40)$$

The results obtained when the eleven runs were optimized together are shown in Figs. 8 and 9. Fig. 8 shows the C_3H_6 and the NO curves, whilst Fig. 9 shows two of the mixed feed experiments, with the parameter values being given in Table 5. Overall the fit is acceptable, but the agreement for the three NO oxidation curves is certainly less good than previously. If it is desired to a model that is valid for mixed feeds only, it is likely a better strategy to use approach one of this paper, that is, optimize only experiments with mixed feed and not bother with trying to obtain a generally perfect model. It is likely that there are coupling terms for the two reactants that are not present in the model.

As a final point, it is interesting to look at the selectivity of the various reactions involving the hydrocarbons. We can define the point selectivity for each of the reactions involving hydrocarbons (one oxidation and three reduction reactions) as the rate of disappearance of propene in each reaction divided by the total rate of disappearance of propene. These calculations were made for the whole reactor and, as an example, the results for Run 16 are shown in Fig. 10. The results shown are point selectivity at a position 20 mm downstream from the reactor entrance. Fig. 10(a) shows the selectivity for oxidation, whilst Fig. 10(b) shows the selectivity for the three reduction reactions. It is clearly seen that at all times most of the propene is being oxidized, and that the maximum selectivity towards reduction occurs at around 480 K. The variation of the selectivity with axial distance and temperature is illustrated in Fig. 11. Clearly, the local selectivity depends on not only temperature, but the local reactant concentrations. To verify the accuracy of these simulations would require an in situ measurement of reactant concentrations by, for example, SpaciMS.

7. Concluding remarks

In this paper we have presented results for experimental and modelling study of the selective catalytic reduction of NO by propene on platinum and platinum/palladium catalysts. The general experimental trends observed are generally in agreement with the literature. Relatively large amounts of N_2O were formed over both catalysts. It was possible to match the experimental results using global type kinetic models of the LHHW form, using previous results from the literature as a starting point in the model development.

Acknowledgements

This work was funded by the Auto21 Networks of Centres of Excellence, and the Natural Science and Engineering Research Council of Canada.

References

- [1] R.M. Heck, R.J. Farrauto, S.T. Gulati, *Catalytic Air Pollution Control, Commercial Technology*, Wiley, New York, 2009.

- [2] J. Pérez-Ramírez, F. Kapteijn, K. Schöffel, J.A. Moulijn, *Applied Catalysis B: Environmental* 44 (2003) 117–151.
- [3] A.G. Konstandopoulos, M. Kostoglou, S. Lorentzou, N. Vlachos, *Catalysis Today* 188 (2012) 2–13.
- [4] T.C. Watling, M.R. Ravenscroft, G. Avery, *Catalysis Today* 188 (2012) 32–41.
- [5] I. Nova, C. Ciardelli, E. Tronconi, D. Chatterjee, M. Weibe, *Topics in Catalysis* 42–43 (2007) 43–46.
- [6] A. Scheuer, A. Drochner, J. Gieshoff, H. Vogel, M. Votsmeier, *Catalysis Today* 188 (2012) 70–79.
- [7] J. Koop, O. Deutschmann, *Applied Catalysis B: Environmental* 91 (2009) 47–58.
- [8] S. Voltz, C. Morgan, D. Liederman, S. Jacob, *Industrial & Engineering Chemistry Product Research and Development* 12 (1973) 294–301.
- [9] S.H. Oh, J.C. Cavendish, L.L. Hegedus, *AIChE Journal* 26 (1980) 935–940.
- [10] S.H. Oh, J.C. Cavendish, *Industrial & Engineering Chemistry Product Research and Development* 21 (1982) 29–30.
- [11] S.H. Oh, J.C. Cavendish, *AIChE Journal* 31 (1985) 935.
- [12] C. Sola, A. Abedi, R.E. Hayes, W.S. Epling, M. Votsmeier, *Canadian Journal of Chemical Engineering* (2013) (in press).
- [13] G.C. Koltsakis, I.P. Kandylas, A.M. Stamatelos, *Three-way catalytic converter modeling and applications*, *Chemical Engineering Communications* 164 (1998) 153–189.
- [14] A. Pandya, J. Mmbaga, R.E. Hayes, W. Hauptmann, M. Votsmeier, *Topics in Catalysis* 52 (2009) 1929–1933.
- [15] K. Hauff, U. Tüttles, G. Eigenberger, U. Niessen, *Applied Catalysis B: Environmental* 100 (2010) 10–18.
- [16] C. Sola-Quiroz, MSc, Department of Chemical and Materials Engineering, University of Alberta, Edmonton, AB, Canada, 2011.
- [17] M. Khosravi-Hafshejani, MSc, Department of Chemical and Materials Engineering, University of Alberta, Edmonton, AB, Canada, 2013.
- [18] C. Sampara, E. Bissett, M. Chmielewski, D. Assanis, *Industrial & Engineering Chemistry Research* 46 (2007) 7993–8003.
- [19] W. Hauptmann, M. Votsmeier, J. Gieshoff, A. Drochner, *Applied Catalysis B: Environmental* 93 (2009) 22–29.
- [20] L. Olsson, E. Fridell, *Journal of Catalysis* 210 (2002) 340–350.
- [21] A. Abedi, R.E. Hayes, M. Votsmeier, W.S. Epling, *Catalysis Letters* 142 (2012) 930–935.
- [22] R.E. Hayes, F.H. Bertrand, C. Audet, S.T. Kolaczkowski, *Canadian Journal of Chemical Engineering* 81 (2003) 1192–1199.
- [23] W. Hauptmann, A. Drochner, H. Vogel, M. Votsmeier, J. Gieshoff, *Topics in Catalysis* 42–43 (2007) 157–160.
- [24] S.S. Mulla, N. Chen, W.N. Delgass, W.S. Epling, F.H. Ribeiro, *Catalysis Letters* 100 (2005) 267–270.
- [25] S.S. Mulla, N. Chen, L. Cumaranatunge, G.E. Blau, D.Y. Zemlyanov, W.N. Delgass, W.S. Epling, F.H. Ribeiro, *Journal of Catalysis* 241 (2006) 389–399.
- [26] D. Bhatia, R.W. McCabe, M.P. Harold, V. Balakotaiah, *Journal of Catalysis* 266 (2009) 106–119.
- [27] W. Held, A. Konig, T. Richter, L. Ruppe, SAE paper No. 900496.
- [28] M. Iwamoto, *Proceedings of Meeting of Catalytic Technology for Removal of Nitrogen Monoxide*, Tokyo, January, 1990, p. 17.
- [29] M.D. Amiridis, T. Zhang, R.J. Farrauto, *Applied Catalysis B: Environmental* 10 (1996) 203–227.
- [30] R. Burch, D. Ottrey, *Applied Catalysis B: Environmental* 13 (1997) 105–111.
- [31] S. Lacombe, J.H.B.J. Hoebink, G.B. Marin, *Applied Catalysis B: Environmental* 12 (1997) 207–224.
- [32] K. Irani, W.S. Epling, R. Blint, *Applied Catalysis B: Environmental* 92 (2009) 422–428.
- [33] R. Burch, D. Ottrey, *Applied Catalysis B: Environmental* 9 (1996) L19–L24.
- [34] G.P. Ansell, P.S. Bennett, J.P. Cox, J.C. Frost, P.G. Gray, A.M. Jones, R.R. Rajaram, A.P. Walker, M. Litorell, G. Smedler, *Applied catalysis B: Environmental* 10 (1996) 183–201.
- [35] R. Burch, T.C. Watling, *Catalysis Letters* 43 (1997) 19–23.
- [36] R. Burch, P.J. Millington, *Catalysis Today* 29 (1996) 37–42.
- [37] R. Burch, T.C. Watling, in: N. Kruse, A. Frennet, J.-M. Bastin (Eds.), *Studies in Surface Science and Catalysis*, vol. 116, Elsevier, 1998, pp. 199–211.
- [38] R. Burch, P. Fornasiero, B.W.L. Southward, *Journal of Catalysis* 182 (1999) 234–243.
- [39] J.A. Sullivan, R. Burch, A.A. Shestov, *Chemical Engineering Research and Design* 78 (2000) 947–953.
- [40] R. Burch, J.P. Breen, F.C. Meunier, *Applied Catalysis B* 39 (2002) 283.
- [41] R. Burch, *Catalysis Today* 35 (1997) 27.
- [42] R. Burch, J.A. Sullivan, T.C. Watling, *Catalysis Today* 42 (1998) 13.